

# A Model Structure for Size-by-Liberation Recoveries in Flotation

Paulina Vallejos <sup>1,2</sup> , Juan Yianatos <sup>1,2</sup> and Luis Vinnett <sup>1,2,\*</sup> 

<sup>1</sup> Department of Chemical and Environmental Engineering, Federico Santa Maria Technical University, Valparaíso 2390123, Chile; paulina.vallejos@usm.cl (P.V.); juan.yianatos@usm.cl (J.Y.)

<sup>2</sup> Automation and Supervision Centre for Mining Industry, CASIM, Federico Santa Maria Technical University, Valparaíso 2390123, Chile

\* Correspondence: luis.vinnett@usm.cl

**Abstract:** This communication presents a model structure for the flotation recovery of middling particles (10–90% liberation). Fourteen datasets from the literature were studied (galena flotation), which involved different flotation systems and operating conditions. The flotation responses allowed the model flexibility to be evaluated under a range of recovery profiles. The modelling results showed that galena recovery can be characterized by the interaction between a linear function and a concave function (e.g., Gamma model), to account for the liberation and particle size effects, respectively. Liberation also impacts the location and dispersion of the recovery dependence on particle size. The proposed model structure showed there was adequate flexibility with five parameters, leading to adjusted coefficients of determination ranging from 0.863 to 0.998 for the studied datasets. Thus, an alternative approach for modelling the recovery of middling particles is proposed, which represents the liberation and particle size dependence with a few parameters.

**Keywords:** size-by-liberation; flotation; mineral recovery; middling particles; modelling



**Citation:** Vallejos, P.; Yianatos, J.; Vinnett, L. A Model Structure for Size-by-Liberation Recoveries in Flotation. *Minerals* **2021**, *11*, 194. <https://doi.org/10.3390/min11020194>

Academic Editors: William Skinner and Lev Filippov

Received: 24 December 2020

Accepted: 2 February 2021

Published: 12 February 2021

**Publisher's Note:** MDPI stays neutral with regard to jurisdictional claims in published maps and institutional affiliations.



**Copyright:** © 2021 by the authors. Licensee MDPI, Basel, Switzerland. This article is an open access article distributed under the terms and conditions of the Creative Commons Attribution (CC BY) license (<https://creativecommons.org/licenses/by/4.0/>).

## 1. Introduction

Flotation performance has proved to be strongly dependent on particle size and liberation. To obtain targeted metallurgical results, mineral particles cannot be excessively fine or coarse due to the typically low flotation rates caused by hydrodynamic cell conditions [1–4]. Mineral liberation also influences the flotation recovery through its relationship with the collection probability and mineral transport in flotation operations. Some attempts have been made to characterize the flotation performance as a function of particle size and liberation. These evaluations have been more common since the introduction of automated mineralogy, with QEMSCAN (Quantitative Evaluation of Minerals by Scanning Electron Microscopy) and MLA (Mineral Liberation Analyzer) being the most utilized systems for the analysis of polished sections.

Modelling of flotation processes has not been straightforward because of random particle features such as size, shape, association, texture, among others. Kinetic models have been used to describe flotation systems, with the flotation rate being a function of particle size, mineralogical properties and operating conditions. Steiner [5] modelled the flotation rate as a function of particle size and degree of locking for the Pb–Zn separation. The associated particles (screened) were analysed by microscopic examination of polished sections. The floatability of particles typically presented the concave trend as a function of particle size reported in the literature, with a shift to the right at higher liberation. Bartlett and Mular [6] studied the flotation of hematite from quartz at  $-48 + 65 \mu\text{m}$ ,  $-65 + 100 \mu\text{m}$ ,  $-100 + 150 \mu\text{m}$ ,  $-150 + 200 \mu\text{m}$  and  $-200 + 270 \mu\text{m}$  and hematite contents of 0–17%, 17–39%, 39–56%, 56–70% and 84–100%. The latter was obtained by dense medium separation (DMS). The results indicated that the rate constant decreased with particle size and increased with hematite content. The rate constant dependence on the particle

composition presented an S-shaped trend. Hill, et al. [7] analysed size-by-composition sphalerite flotation in a pilot-scale column (cleaner stage). Three size classes were studied:  $-13 + 9 \mu\text{m}$ ,  $-37 + 13 \mu\text{m}$  and  $+37 \mu\text{m}$ . The particle compositions were obtained by a scanning electron microscope in backscattered electron imaging mode. The estimated rate constants presented an approximately linear increasing trend with particle composition. Vianna [8] studied the size-by-liberation galena flotation in a laboratory-scale continuous flotation cell. Five size classes were analysed:  $-150 + 106 \mu\text{m}$ ,  $-106 + 75 \mu\text{m}$ ,  $-75 + 38 \mu\text{m}$ ,  $-38 + 20 \mu\text{m}$  and  $-20 + 10 \mu\text{m}$ . MLA was used to characterize galena liberation. At fixed particle sizes and collector concentrations, the floatability of galena increased (non-linearly) with liberation. The non-linearity was mainly caused by the flotation responses of the high and low-liberated particles. The rate constants in the studied liberation classes presented the typical concave pattern as a function of the particle size, with higher amplitudes at higher liberation. Similar size-by-liberation results were obtained by Welsby [9] and Welsby, et al. [10] for the flotation of galena. The rate constant decreased in the finer ( $-19 \mu\text{m}$ ) and coarser ( $+75 \mu\text{m}$ ) size classes and for low-liberated particles. Jameson [4] analysed Welsby's data to evaluate the effect of particle size and liberation on the rate constant. The results showed that the ratio between the rate constant (of unliberated particles) and the maximum rate constant (for fully liberated particles) was independent of particle size. The poor recovery of coarse particles was not entirely justified by poor liberation, being mainly attributable to hydrodynamic conditions in the flotation cell. More recently, Alves dos Santos [11] modelled chalcopyrite recovery in terms of surface liberation and particle size. The surface liberation was estimated from the chalcopyrite content, assuming sphere-equivalent particles and surface liberation being proportional to the mineral grade. The results showed that the ratio between the recovery and the chalcopyrite surface area in the feed was linearly related to particle size for particles with more than 15% of chalcopyrite.

This communication presents a model structure for the size-by-liberation flotation recovery of middling particles in the ranges of 10–90% liberation and 0–150  $\mu\text{m}$ . Middling particles are commonly studied because most of the difficulties in flotation are related to the treatment of these particles [12], as liberated particles are easily recovered and locked particles typically have less chance of recovery in the flotation process. Although some ores may present more erratic responses at higher liberation (e.g., 20% instead of 10%) and significantly faster responses from lower upper bounds (e.g., 80% instead of 90%), the proposed model structure allowed galena recovery to be described for a liberation range of between 10% to 90%. This range can be changed depending upon the flotation response, given the ore/mineral characteristics and operating conditions. It should be noted that the content of middling particles has increased in industrial operations due to the increase in feed tonnage to compensate for lower feed grades, which consequently decreases the mineral liberation. The size-by-liberation recoveries reported by Vianna [8], Savassi [13] and Welsby [9] were studied, in which the cross-sectional galena compositions were obtained by QEM\*SEM (Quantitative Evaluation of Minerals by Scanning Electron Microscopy) or MLA as estimates for liberation from polished sections. Savassi [13] stated that areal grades are measured from these sections, which justifies stereological corrections for transformation to volumetric bases. Ueda, et al. [14] performed simulations using discrete elements methods to study the effect of the number of analysed particles on the dispersion and reliability of the liberation estimates. The results showed that processing a larger number of particles reduces the dispersion in the 2D liberation (areal grade); however, stereological biases are always present when 3D liberation (volumetric grade) is estimated from 2D measurements. Surface exposure of valuable minerals as well as other 3D particle characteristics can be also analysed using X-ray microCT (XMT) as described by Lin and Miller [15], Miller, et al. [16], and Reyes, et al. [17]. No stereological corrections were conducted in this communication, which implies that the modelling results are applicable to liberation measurements based on 2D data.

## 2. Experimental Data and Methodology

Size-by-liberation data reported by Vianna [8], Savassi [13] and Welsby [9] were analysed. The former and the latter were obtained in single continuous laboratory cells using MLA, whereas Savassi's data were obtained in a continuous industrial operation using QEM\*SEM. The results reported by Savassi [13] allowed not only the characterization of single flotation cells, but also of an industrial flotation bank (rougher). These studies focused on investigating the effect of particle size and liberation (cross-section composition) on galena floatability. Between 2000 and 7000 particles per sample were analysed by MLA or QEM\*SEM [8,9,13]. Thus, the size-by-liberation recoveries were obtained. Vianna [8] and Welsby [9] also studied the effect of collector dosages on the flotation response. Table 1 shows the flotation systems, minerals involved, collector types and concentrations, and the liberation analyses performed on the flotation products. The experimental conditions considered particle sizes of  $-150 \mu\text{m}$  and collector dosages from 5 to 40 ppm. For further details on the experimental procedures, please refer to [8–10,13,18].

**Table 1.** Summary of experimental conditions, flotation feed and liberation analyses.

Flotation System		Minerals	Liberation Analyses	Collector Type and Concentration g/ton	Size Classes, $\mu\text{m}$
Vianna [8,18]	One 3-L cell, continuous operation	Galena, sphalerite and NSG *	MLA	Aerophine 3418A, 5, 7.5, 10, 15, 30 g/ton	$-150 + 106$ , $-106 + 75$ , $-75 + 38$ , $-38 + 20$ , $-20 + 10$
Savassi [13]	12 cells, industrial circuit	Galena, sphalerite, pyrite and NSG *	QEM*SEM	Ethyl Xanthate, non-specified concentration	$-75 + 53$ , $-28 + 20$ , $-20 + 14$ , $-10 + 14$
Welsby [9,10]	One 40-L cell, continuous operation	Galena, sphalerite and NSG *	MLA	Sodium Ethyl Xanthate, 5, 15, 40 g/ton	$+106$ , $-106 + 75$ , $-75 + 38$ , $-38 + 28$ , $-28 + 19$ , $-19 + 10$ , $-10$

(\*) NSG: Non-Sulphide Gangue; CS: Cyclosizer.

A model structure for the size-by-liberation recoveries of galena was defined and evaluated. The 10–90% liberation classes were studied due to their increasing presence in industrial applications. These particles typically present slower flotation responses than fully liberated particles and significantly higher recoveries than locked particles. The recovery dependences on liberation and particle size were first studied, which allowed a general model structure to be determined and assessed. In all cases, the model parameters were obtained by least-squares estimation.

## 3. Recovery Dependence on Liberation and Particle Size

### 3.1. Effect of Liberation on Galena Recovery

Recovery ( $R$ ) of middling particles has shown to be well-described by increasing trends as a function of liberation ( $L$ ) at constant particle sizes ( $d_p$ ) and experimental conditions [4,7]. These increasing trends were consistently observed in the evaluated flotation systems for different collector dosages, particle sizes, residence times and cell numbers (in the industrial flotation bank). Figure 1 illustrates the typical relationship observed for the liberation–recovery at constant experimental conditions. Figure 1a shows Vianna's results at a collector dosage of 15 g/ton, Figure 1b the rougher recoveries reported by Savassi [13] (10 cells in series) and Figure 1c Welsby's results at a collector dosage of 15 g/ton. The cumulative recoveries were analysed for the rougher flotation circuit [Figure 1b]. The experimental data are presented as dispersion datapoints. All reported size classes are presented. The 10–90% liberation classes approached a linear trend, as detailed in Figure 1, with a minimum  $R^2_{adj}$  of 0.80. Thus, Equation (1) was proposed to describe the recovery dependence as a function of liberation at a constant particle size and collector concentration:

$$R(L) = \alpha \cdot L + \beta \quad (1)$$

where  $\alpha$  and  $\beta$  are fitting parameters. The  $\alpha$  value estimates the recovery increase per liberation unit at a constant particle size, whereas parameter  $\beta$  defines the recovery offset caused by the particle size dependence. It should be mentioned that  $L$  was estimated from

the cross-sectional composition of the polished samples. The linear fitting is presented in Figure 1 as continuous lines. Potential and exponential growth was also evaluated; however, these trends did not show consistent improvements with respect to Equation (1).

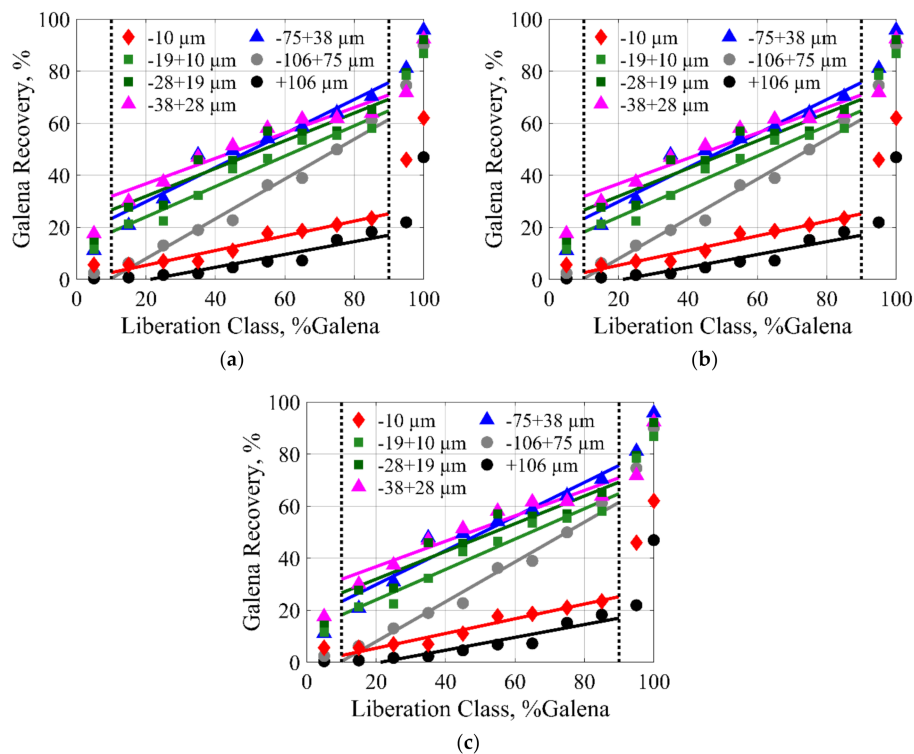


**Figure 1.** Galena recoveries versus liberation: (a) Vianna [8] 15 g/ton of Aerophine 3418A, (b) Savassi [13] 10 cells in series, and (c) Welsby [9] 15 g/ton of Sodium Ethyl Xanthate Experimental data are presented as datapoints and model fitting as the trend line. The vertical lines define the validity range for the linear trends.

The size-by-liberation recoveries reported by Vianna typically presented flatter profiles across the studied liberation and size classes. The ore characteristics, flotation machine and operating conditions may have rendered the flotation responses less sensitive to the particle features, leading to comparable recoveries (by liberation) in the  $-10 + 20 \mu\text{m}$  and  $-150 + 106 \mu\text{m}$  size classes.

Results of Figure 1 indicate that the mineral recovery, which is related to the particle-bubble aggregate formation, has an approximately linear dependency on liberation. Mineral liberation, measured from the cross-sectional composition, was assumed to be proportional to surface exposure, which directly impacts the mineral recovery. It should be noted that the slopes and intercepts in Figure 1 depended upon the particle size, collector concentration and flotation system.

### 3.2. Effect of Particle Size on Galena Recovery

Mineral recovery strongly depends on particle size, with fine and coarse particles having lower recoveries due to hydrodynamic constraints. The concave relationship between recovery and particle size has been widely documented by several authors [1,3,8,9]. Different model structures for the recovery as a function of particle size (at constant liberation and collector concentrations) were studied. The datasets detailed in Table 1 were again analysed. The concavities of some probability density functions (PDF) were considered to define the model structure for the recovery as a function of particle size. Thus, the Log-normal, Weibull and Gamma PDFs were compared. These curves were denormalized

to describe the entire range of recoveries. The best performance was obtained with the Gamma model of Equation (2):

$$R(d_P) = c \cdot \frac{1}{\Gamma(a_G) \cdot d_G^{a_G}} \cdot d_P^{a_G-1} \cdot \exp\left(-\frac{d_P}{d_G}\right) = C \cdot d_P^{a_G-1} \cdot \exp\left(-\frac{d_P}{d_G}\right) \quad (2)$$

where  $a_G$  and  $d_G$  correspond to the shape and scale parameters,  $\Gamma(a_G)$  is the Gamma function and  $c$  allows the denormalization. Within Equation (2), the constant terms were replaced by parameter  $C$ . The Gamma model has then three parameters, with adequate flexibility to represent a wide range of shapes.

Figure 2 illustrates the recovery as a function of particle size at constant collector dosages and liberation. The x-axes are presented in logarithmic scale. All liberation classes in the range 10–90% are presented. Figure 2a–c shows Vianna’s results at a collector dosage of 15 g/ton, Savassi’s results for 10 cells in series and Welsby’s results at a collector dosage of 15 g/ton, respectively. The experimental data are presented as dispersion datapoints and the model fitting as continuous lines. The Gamma model allowed the different shapes to be described using three parameters, with a minimum  $R_{adj}^2$  of 0.52. Lower  $R_{adj}^2$  values were obtained with Vianna’s data due to the flatter recovery profiles and the low number of degrees of freedom. Three aspects can be highlighted from Figure 2:

- Higher recoveries were consistently observed at higher liberation, which increased  $C$  in Equation (2).
- The shapes of the particle size–recovery curves did not change significantly at different liberations, which implied non-significant  $a_G$  changes in Equation (2).
- The particle size–recovery curves shifted to the right and broadened at higher liberation, which can be obtained by increasing the mean value and standard deviation of the Gamma model.

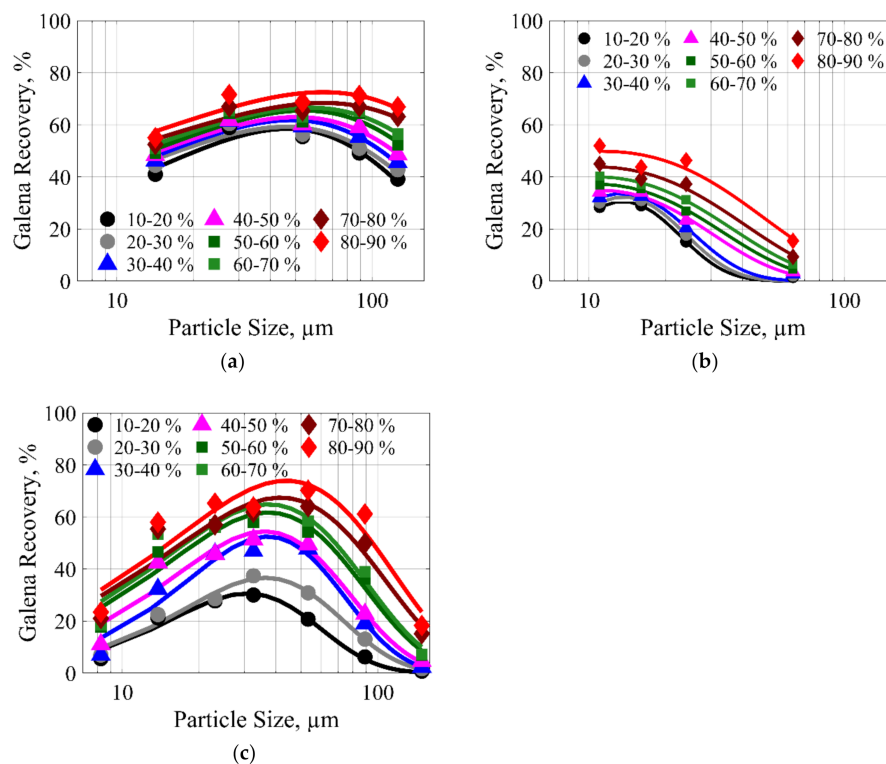


**Figure 2.** Galena recoveries versus particle size: (a) Vianna [8] 15 g/ton of Aerophine 3418A, (b) Savassi [13] 10 cells in series, and (c) Welsby [9] 15 g/ton of Sodium Ethyl Xanthate. Experimental data are presented as datapoints and model fitting as trend line. X-axes in logscale.

The shifts to the right along with the broader curves at higher liberation are consistent with the size-by-composition flotation rates reported by Steiner [5]. It should be noted that the data reported by Savassi [13] did not present the typical concave curves reported in literature. This result considered CS4 as the finest size class (CS: Cyclosizer) and may have been favoured by finer galena grains with respect to Vianna's and Welsby's ores, leading to lower liberation towards the coarser classes. The Gamma model showed sufficient flexibility to fit these recovery decays (Figure 2b).

### 3.3. General Model for the Size-by-Liberation Recovery of Galena

From the results of Figures 1 and 2, a general model structure was defined to describe the size-by-liberation recoveries. The Gamma model showed adequate flexibility to represent the experimental data; however, the parameters proved to be dependent on liberation. Results of Figure 2 indicated that the recovery as a function of particle size increased at higher liberation, which was observed as higher C values in Equation (2). The increase in the C value was consistent with the linear recovery dependence on liberation at constant particle size [Equation (1)]. Higher liberation also shifted and widened the particle size-recovery curves. For a Gamma model, the mean value  $d_{mean}$  and standard deviation  $\sigma_d$  are given by

$$\begin{aligned} d_{mean} &= a_G \cdot d_G \\ \sigma_d &= \sqrt{a_G} \cdot d_G \end{aligned} \quad (3)$$

As the shape of the concave curves of Figure 2 did not change significantly (i.e.,  $a_G$  approximately constant), a  $d_G$  increase as a function of liberation [Equation (3)] shifts the location of the concave curve to the right, also increasing the dispersion. Different  $d_G$  dependences on liberation were evaluated, with exponential growth being the model structure that led to satisfactory results for the experimental data detailed in Table 1. Equation (4) was then proposed to fit the size-by-liberation recoveries:

$$\begin{aligned} R(d_P) &= (\alpha \cdot L + \beta) \cdot d_P^{a_G-1} \cdot \exp\left(-\frac{d_P}{d_G}\right) \\ d_G &= \delta \cdot \exp(\lambda \cdot L) \end{aligned} \quad (4)$$

where  $\delta$  and  $\lambda$  are additional fitting parameters. The model structure of Equation (4) was again evaluated from Vianna's, Savassi's and Welsby's datasets, which involved 40, 32 and 56 size-by-liberation recoveries per experimental condition, respectively. The five model parameters ( $\alpha$ ,  $\beta$ ,  $a_G$ ,  $\delta$ ,  $\lambda$ ) were estimated by non-linear regression.

## 4. Modelling Results

The ability of Equation (4) to describe size-by-liberation recoveries was studied from fourteen datasets reported by Vianna [8], Savassi [13], and Welsby [9]. Different systems, feed properties and reagent schemes are considered in these datasets such as: laboratory (3 L and 40 L) and plant scale flotation machines, different particle size distributions, reagent types and dosages, size and liberation classes and others. Thus, the model flexibility was evaluated under a wide range of experimental conditions. Figure 3 presents the size-by-liberation recoveries and model fitting for Vianna's [(a) and (b)], Savassi's [(c) and (d)] and Welsby's [(e) and (f)] middling data. These experimental data are depicted as datapoints, whereas the model fitting is presented as 3D surfaces. The particle size axes are presented in logarithmic scale. The colormaps are referential, with blue and yellow representing the minimum and maximum values respectively, in each experimental condition. The best (left) and worst (right) model fitting per dataset are shown, based on the adjusted coefficient of determination  $R_{adj}^2$ . These extreme conditions coincided with the lowest and highest recovery profiles per dataset. Conditions with lower recoveries typically presented flatter size-by-liberation dependence, which favoured the model fitting. A good agreement between the experimental and modelled recoveries was typically obtained, with  $R_{adj}^2$  ranging from 0.863 to 0.998. Thus, the proposed model structure showed adequate flexibility to describe the recovery variability caused by differences in particle size and liberation

(10–90%) at different collector concentrations and number of cells in series. It should be noted that this flexibility was achieved with only five model parameters for experimental conditions with 40, 32 and 56 size-by-liberation recoveries. Comparisons of Figure 3a,b, and Figure 3e,f, show significant recovery increases in the more liberated categories and intermediate particle sizes (20–60  $\mu\text{m}$ ) when increasing the collector dosage. Figure 3a,b also show a significant improvement in the recovery of coarse and highly liberated particles (100–150  $\mu\text{m}$ ) at higher collector concentrations, in agreement with the results reported by Fosu, et al. [19].

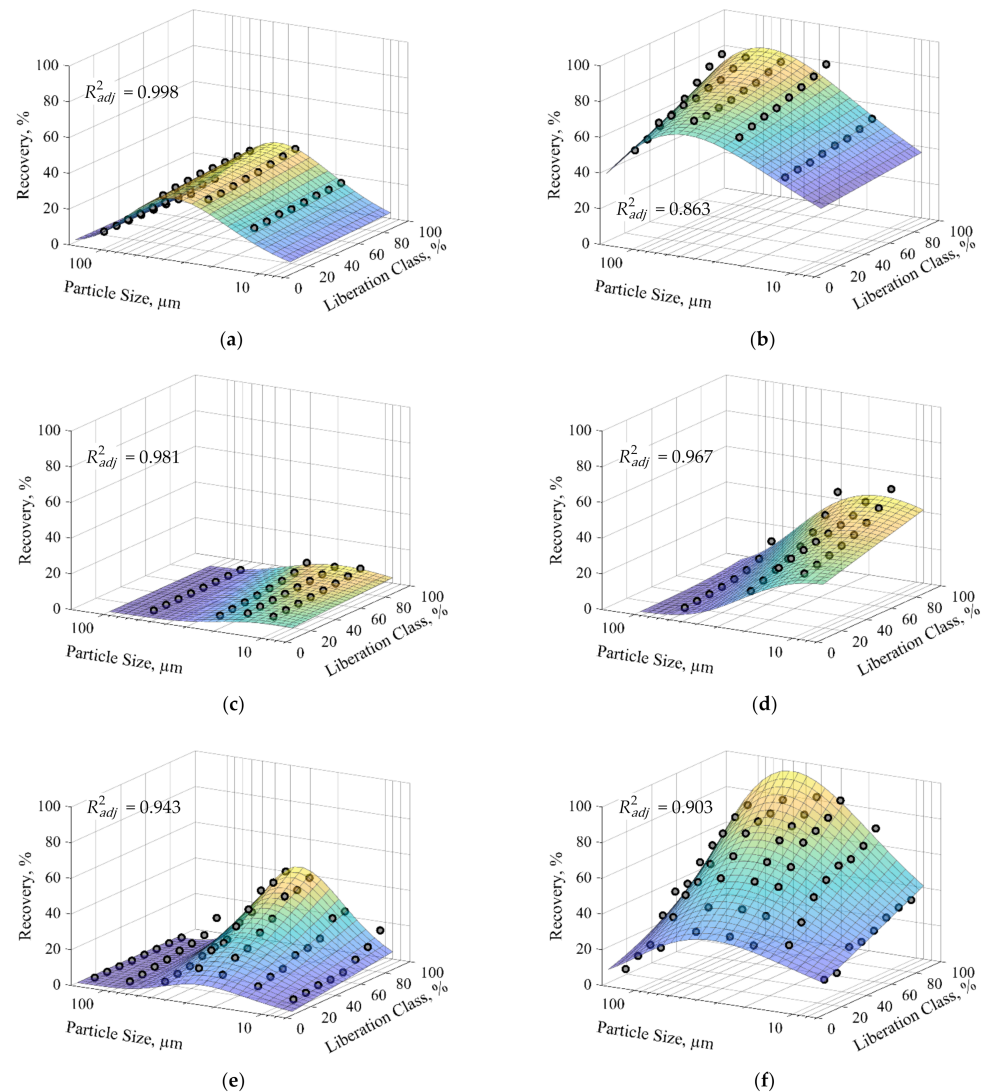


**Figure 3.** Size-by-liberation galena recoveries and model fitting: Vianna [8] (a) 5 g/ton of Aerophine 3418A, (b) 30 g/ton of Aerophine 3418A; Savassi [13] (c) 2 cells in series, (d) 12 cells in series; and Welsby [9] (e) 5 g/ton of Sodium Ethyl Xanthate, (f) 40 g/ton of Sodium Ethyl Xanthate. Experimental data are presented as datapoints and model fitting as 3D surfaces. Middling particles (10–90% liberation). Particle size axes are in logscale.

Figure 4 compares all the measured and model recoveries per dataset [(a) Vianna’s data, (b) Savassi’s data and (c) Welsby data]. The proposed model structure allowed a wide range of size-by-liberation recoveries to be represented. The model fitting presented higher variability with Welsby’s [Figure 4c] data due to the higher number of datapoints. The deviations between the modelled and measured recoveries were typically more significant at higher recoveries. These differences can be observed in Figures 2 and 3 in the vicinity of

the maxima. Thus, a model structure with flatter size dependence close to the maximum may potentially improve the model fitting. However, attention must be paid to over-fitting, especially when the number of parameters approaches the number of datapoints. The 95% prediction intervals for the results of Figure 3 are presented in Appendix A. These intervals were not overlapped between the extreme recovery values, showing that the model can represent adequately the recovery variability.

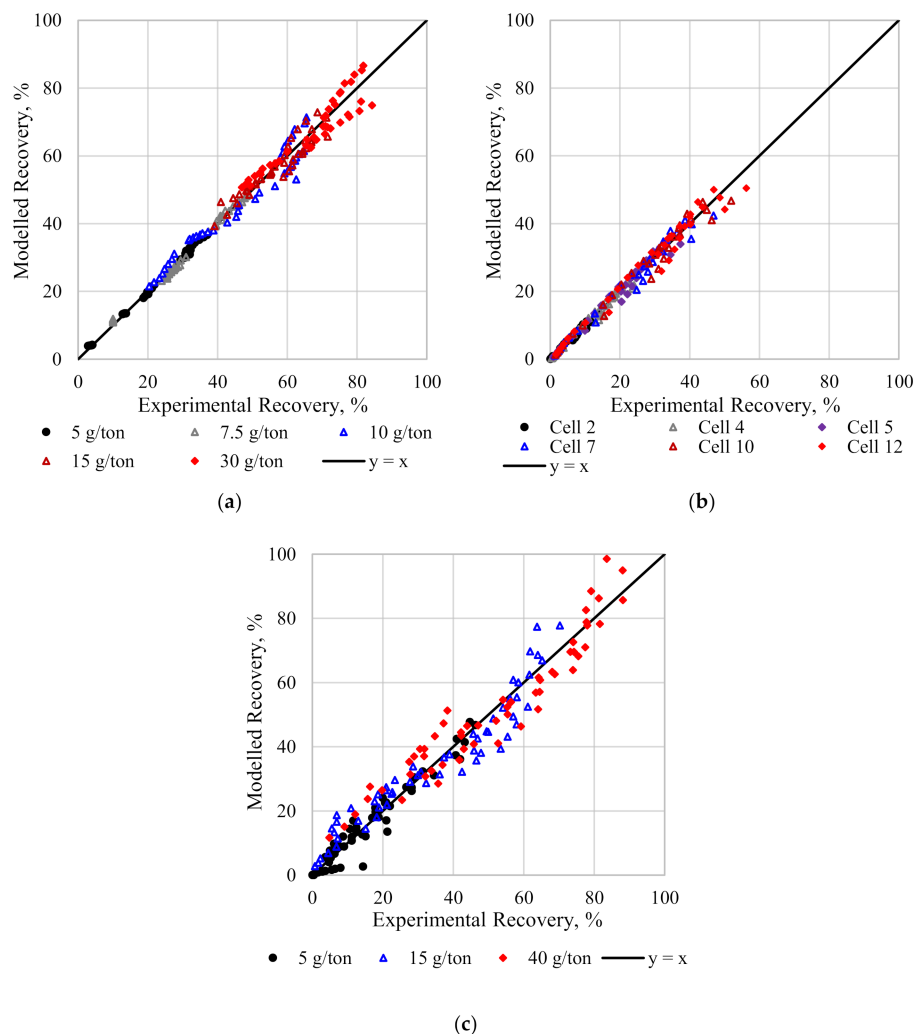


**Figure 4.** Comparison between measured and modelled size-by-liberation galena recoveries: (a) Vianna [8], (b) Savassi [13], (c) Welsby [9]. Middling particles (10–90% liberation).

The proposed model structure for the size-by-liberation recovery of middling particles showed adequate performance to describe 14 datasets under different experimental conditions. The results of Figure 3 indicate that the modelling procedure can be applied to specific flotation systems, such as those detailed in Table 1. The model applicability in flotation systems with narrower linear dependence as a function of liberation can be bounded to narrower middling ranges. Alternative increasing trends can be also evaluated (e.g., potential or exponential growth) for moderate recovery increases towards the liberated classes. The Gamma term will be typically more robust due to its flexibility to represent a wide range of mound-shaped patterns. Exceptions are concave trends with negative skewness or with an approximately flat response around the maximum, for which additional model parameters are required. The size-by-liberation recoveries analysed here may have been subject to significant bias, especially in the  $-20 \mu\text{m}$  classes due to system resolution, sample preparation and aggregation. The model performance under more

accurate recovery estimates can be improved or worsened depending upon changes in the liberation–recovery relationship and the concave trend with particle size. The increasing liberation–recovery relationship can be bounded to shorter middling ranges or modified to other growth curves. The concave relationship will be less sensitive to these corrections due to its flexibility to represent monotonic and mounded functions. The middling recoveries may also be used to describe kinetic responses and identify typical changes in the size-by-liberation recoveries as a function of time. For example, the slow-floating particles may present significantly different responses as time progresses, with some of them reaching a plateau after some flotation intervals and some of them presenting sustained increasing recoveries. Thus, the modelled recoveries will tend to increase and/or remain unchanged over time in different size-by-liberation categories. This application is particularly useful when simulating flotation processes with the aim of estimating losses at the end of the process. Further developments must be made to include liberated and locked particles in the modelling scheme. In addition, the parameter dependence on different experimental conditions and feed properties will allow for the development of generalized models for prediction purposes.

## 5. Conclusions

A simple model structure to describe the flotation recovery of middling particles was presented. The model was evaluated from 14 size-by-liberation datasets reported in the literature, which presented different flotation responses for galena separation. The main results are summarized as follows:

- A linear trend showed adequate performance to describe the recovery increase with liberation for middling particles (liberation classes between 10% and 90%), at constant particle size.
- The concave recovery dependence on particle size at constant liberation was represented by a Gamma model. The location and dispersion of the concave trend was a function of liberation, which was incorporated through the scale parameter of the Gamma model.
- The proposed model structure considered the combined effect of liberation (linear) and particle size (concave). The model showed suitable flexibility to fit the 14 evaluated size-by-liberation datasets, using five parameters.
- Adequate model fitting was obtained with adjusted coefficient of determinations ranging from 0.863 to 0.998 for all datasets.

Work is under development to model the recovery of liberated (>90%) and locked particles (<10%) for the full range of particle sizes.

**Author Contributions:** Methodology, P.V. and J.Y.; Software, L.V.; Formal Analysis, P.V.; Writing—Original Draft Preparation, P.V., J.Y. and L.V.; Writing—Review & Editing, P.V., J.Y. and L.V.; Supervision, J.Y. and L.V.; Project Administration, J.Y.; Funding Acquisition, J.Y. and L.V. All authors have read and agreed to the published version of the manuscript.

**Funding:** The authors are grateful to Agencia Nacional de Investigación y Desarrollo (ANID), Project Fondecyt 1201335, and Federico Santa Maria Technical University for providing funding for process modelling and control research. S.D.D. Welsby and S.M.S.M. Vianna are also acknowledged for authorizing the use of their unpublished data.

**Institutional Review Board Statement:** Not applicable.

**Informed Consent Statement:** Not applicable.

**Conflicts of Interest:** The authors declare no conflict of interest.

## Appendix A

Figure A1 shows the 95% prediction intervals for the size-by-liberation models depicted in Figure 3. The recovery variability as a function of particle size and liberation was adequately described. Higher uncertainties were observed at higher mean squared errors

(and lower  $R^2_{adj}$ ). However, these uncertainties did not overlap the prediction intervals of the lowest and highest recoveries.

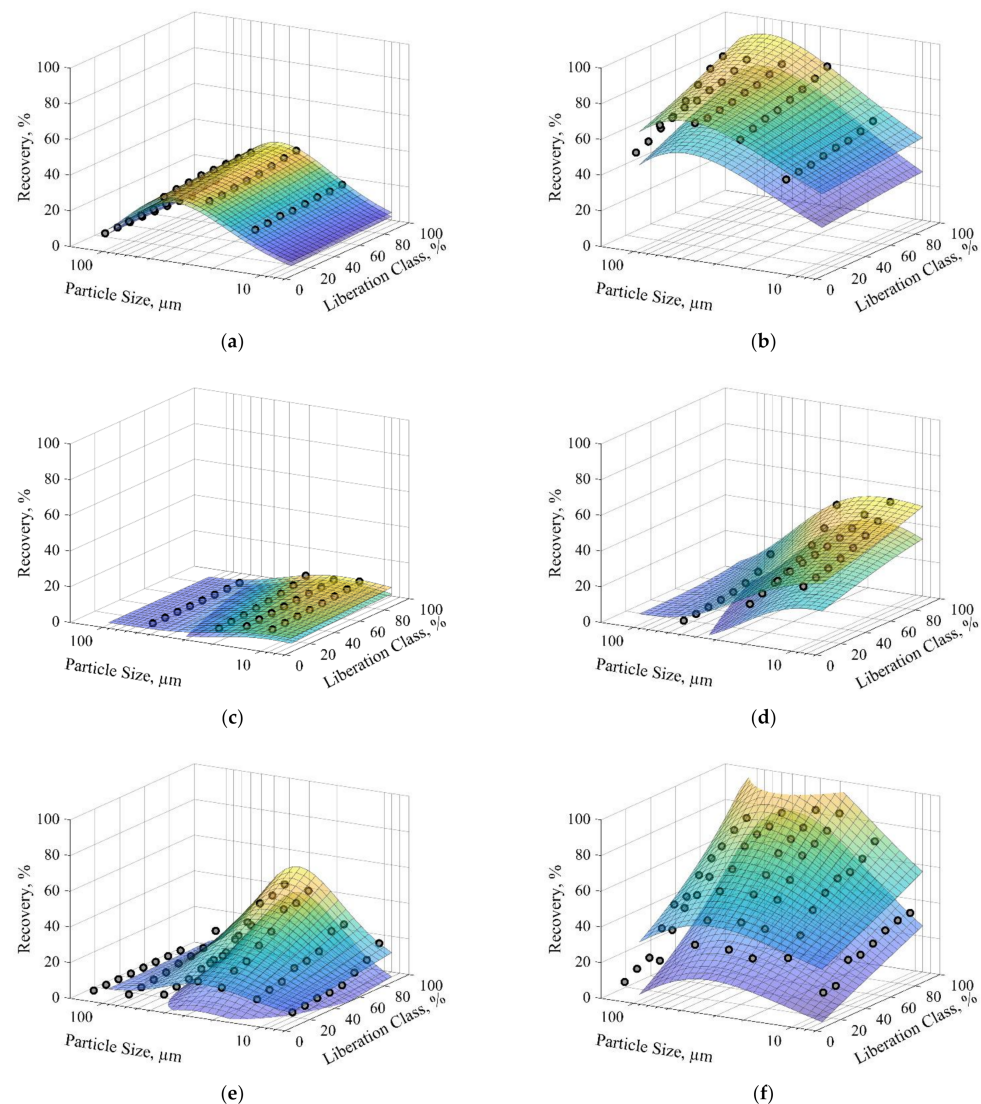


**Figure A1.** 95% prediction intervals for the size-by-liberation galena recoveries: Vianna [8] (a) 5 g/ton of Aerophine 3418A, (b) 30 g/ton of Aerophine 3418A; Savassi [13] (c) 2 cells in series, (d) 12 cells in series; and Welsby [9] (e) 5 g/ton of Sodium Ethyl Xanthate, (f) 40 g/ton of Sodium Ethyl Xanthate. Experimental data are presented as datapoints and prediction intervals as 3D surfaces. Middling particles (10–90% liberation). Particle size axes are in logscale.

## References

1. Trahar, W.J. The selective flotation of galena from sphalerite with special reference to the effects of particle size. *Int. J. Miner. Process.* **1976**, *3*, 151–166. [[CrossRef](#)]
2. Trahar, W.J. A rational interpretation of the role of particle size in flotation. *Int. J. Miner. Process.* **1981**, *8*, 289–327. [[CrossRef](#)]
3. Gaudin, A.M.; Groh, J.O.; Henderson, H.B. *Effect of Particle Size on Flotation*; Technical Publication No 414; The American Institute of Mining and Metallurgical Engineers: New York, NY, USA, 1931; pp. 3–23.
4. Jameson, G.J. The effect of surface liberation and particle size on flotation rate constants. *Miner. Eng.* **2012**, *36–38*, 132–137. [[CrossRef](#)]
5. Steiner, H.J. Kinetic aspects of the flotation behaviour of locked particles. In Proceedings of the 10th International Mineral Processing Congress, London, UK, 2–6 April 1973; pp. 653–666.
6. Bartlett, D.R.; Mular, A.L. Dependence of flotation rate on particle size and fractional mineral content. *Int. J. Miner. Process.* **1974**, *1*, 277–286. [[CrossRef](#)]

7. Hill, G.; Rowlands, N.; Finch, J. Circuit analysis and flotation kinetics at Brunswick Mining and Smelting. In *Production and Processing of Fine Particles*; Elsevier: Montreal, QU, Canada, 1988; pp. 47–57.
8. Vianna, S.M.S.M. The Effect of Particle Size, Collector Coverage and Liberation on the Floatability of Galena Particles in an Ore. Ph.D. Thesis, Department of Mining, Minerals and Materials Engineering, The University of Queensland, Brisbane, Australia, 2004.
9. Welsby, S.D.D. On the Interpretation of Floatability Using the Bubble Load. Ph.D. Thesis, The University of Queensland, Brisbane, Australia, 2009.
10. Welsby, S.D.D.; Vianna, S.M.S.M.; Franzidis, J.-P. Assigning physical significance to floatability components. *Int. J. Miner. Process.* **2010**, *97*, 59–67. [[CrossRef](#)]
11. Alves dos Santos, N. Modelling flotation per size liberation class—Part 3—Modelling recoveries using particle surface area. *Miner. Eng.* **2018**, *129*, 15–23. [[CrossRef](#)]
12. Kelly, E.G.; Spottiswood, D.J. *Introduction to Mineral Processing*; John Wiley & Sons: New York, NY, USA, 1982.
13. Savassi, O.N. Estimating the recovery of size-liberation classes in industrial flotation cells: A simple technique for minimizing the propagation of the experimental error. *Int. J. Miner. Process.* **2006**, *78*, 85–92. [[CrossRef](#)]
14. Ueda, T.; Oki, T.; Koyanaka, S. Statistical effect of sampling particle number on mineral liberation assessment. *Miner. Eng.* **2016**, *98*, 204–212. [[CrossRef](#)]
15. Lin, C.L.; Miller, J.D. 3D characterization and analysis of particle shape using X-ray microtomography (XMT). *Powder Technol.* **2005**, *154*, 61–69. [[CrossRef](#)]
16. Miller, J.D.; Lin, C.-L.; Hupka, L.; Al-Wakeel, M.I. Liberation-limited grade/recovery curves from X-ray micro CT analysis of feed material for the evaluation of separation efficiency. *Int. J. Miner. Process.* **2009**, *93*, 48–53. [[CrossRef](#)]
17. Reyes, F.; Lin, Q.; Cilliers, J.; Neethling, S. Quantifying mineral liberation by particle grade and surface exposure using X-ray microCT. *Miner. Eng.* **2018**, *125*, 75–82. [[CrossRef](#)]
18. Vianna, S.M.; Franzidis, J.P.; Manlapig, E.V.; Silvester, E.; Ping-Hao, F. The Influence of Particle Size and Collector Coverage on the Floatability of Galena Particles in a Natural Ore. In Proceedings of the XXII International Mineral Processing Congress, Cape Town, South Africa, 29 September–3 October 2003; pp. 816–826.
19. Fosu, S.; Pring, A.; Skinner, W.; Zanin, M. Characterisation of coarse composite sphalerite particles with respect to flotation. *Miner. Eng.* **2015**, *71*, 105–112. [[CrossRef](#)]